Annual and Seasonal Glacier Mass Balance on Shodug Glacier 2025–2026

Cryosphere Services Division

National Centre for Hydrology and Meteorology

2026

Prepared by:

Arun Puri, Hydro-met officer, apuri@nchm.gov.bt

Phuntsho Tshering, Principal Hydro-met officer, ptshering@nchm.gov.bt

Tshewang Jamtsho, Hydro-met officer, tjamtsho@nchm.gov.bt

Amber Bdr. Rana, Hydro-met officer, abrana@nchm.gov.bt

Published by: National Centre for Hydrology and Meteorology, Royal Government of Bhutan

PO Box: 2017

Thimphu, Bhutan

List of Acronyms:

- HKH – Hindu Kush Himalaya
- WGMS – World Glacier Monitoring Service
- WMO – World Meteorological Organization
- MSI – Multispectral Instrument
- RTK – Real-Time Kinematic
- GNSS – Global Navigation Satellite System
- mm w. e. a^{-1} – Millimeter Water Equivalent per Annum
- DEM – Digital Elevation Model
- IDW – Inverse Distance Weighting
- AGMB – Annual Glacier Mass Balance
- CGMB – Cumulative Glacier Mass Balance
- ICIMOD – International Centre for Integrated Mountain Development
- TCS7 – Trimble Controller Series 7
- WGS 84 – World Geodetic System 1984
- CSV – Comma-Separated Values
- IPCC – Intergovernmental Panel on Climate Change
- UNESCO – United Nations Educational, Scientific and Cultural Organization
- Gt – Gigatonnes
- m. a. s. l. – meters above sea level

List of Figures

List of Tables

Executive Summary

This technical report presents the annual and seasonal glacier mass-balance assessment of Shodug Glacier for the 2025–2026 monitoring period. The study builds on the earlier Shodug Glacier geodetic mass-balance assessments for 2022–2024 and 2024–2025, while extending the seasonal monitoring framework initiated through the NCHM–ICIMOD collaboration in 2025.

The annual glacier-wide mass balance of Shodug Glacier for May 2025–May 2026 was estimated using the in situ geodetic method based on repeat dGPS/RTK GNSS surface-elevation surveys, IDW interpolation, DEM-supported hypsometry, 50 m elevation-band aggregation, and area-weighted integration. The annual geodetic mass balance was -1769.48 ± 306.329 mm w.e. a^{-1}, indicating continued negative mass balance and substantial net glacier mass loss during the 2025–2026 observation year. The annual elevation-difference distribution showed a mean surface lowering of -1.88 m, with the strongest thinning observed in the lower elevation bands and reduced thinning toward higher elevations.

For the November 2025–May 2026 seasonal/winter period, the seasonal mass balance was estimated using the geodetic method. The seasonal geodetic mass balance was +80.60 ± 82.67 mm w.e. The geodetic seasonal balance is slightly positive, reflecting winter snow accumulation and surface-height increase.

The seasonal closure provides an important consistency check on the annual result. The previously reported May–November 2025 seasonal geodetic balance was -1876.70 mm w.e. When combined with the November 2025–May 2026 geodetic balance of +80.60 mm w.e., the seasonal sum is -1796.10 mm w.e. This is close to the annual geodetic balance of -1769.48 mm w.e. a^{-1}, with a residual difference of approximately 26.62 mm w.e., which is small relative to the annual uncertainty. This agreement indicates that the two seasonal components provide a reasonable closure of the annual geodetic mass-balance signal, while also showing that the winter/November–May gain was not sufficient to offset the stronger May–November mass loss.

Terminus mapping shows that Shodug Glacier continued to retreat during the 2025–2026 monitoring period. The measured retreat distances ranged from 3.20 m to 27.20 m, with a mean terminus recession of 12.55 m. The cumulative terminus recession from 2022 to 2026 was

estimated at 76.24 m, providing geometric evidence of continued glacier shrinkage. The mapped glacier area used for the 2025–2026 assessment was approximately 1.110 km², equivalent to 1,110,155 m², and this glacier outline was used to support DEM clipping, hypsometry derivation, and area-weighted mass-balance integration.

A direct annual mass balance could not be calculated for May 2025–May 2026 because the glacier stakes installed in May 2025 were not recovered during the May 2026 field visit, as they were buried under snow. Therefore, the annual balance for 2025–2026 is reported only from the geodetic method.

The principal uncertainties in this assessment arise from elevation-band variability, glacier boundary delineation, dGPS/DEM processing, snow-depth modelling, and the assumed densities of ice and snow. The spatial interpretation is also limited by the distribution of dGPS survey tracks. Despite these limitations, the results provide a consistent continuation of Shodug Glacier monitoring and demonstrate the value of annual geodetic surveys observations for understanding glacier mass change in Bhutan.

Table of Contents

1 Introduction

Mountain glaciers are sensitive indicators of climate variability and change, as their mass balance responds directly to changes in air temperature, snowfall, radiation, and the timing of accumulation and ablation. Global assessments have shown continued glacier mass loss across most mountain regions, with important implications for sea-level rise, downstream water availability, and high-mountain environments (Zemp et al., 2019; Hugonnet et al., 2021; WMO, 2025). In the Hindu Kush Himalaya, glacier change is spatially variable, but the overall trend shows continued glacier thinning and retreat, particularly for smaller and debris-free glaciers (Azam et al., 2018). Glacier mass balance therefore remains one of the most important parameters for assessing glacier health and for understanding the response of mountain cryosphere systems to climate forcing. In this report, mass-balance terminology follows the standardized framework of Cogley et al. (2011), in which glacier mass balance refers to the change in glacier mass over a specified period and can be assessed using different approaches, including geodetic and glaciological methods.

Bhutan contains approximately 700 glaciers, covering about 630 km² of glacierized area, and these glaciers are important for sustaining river flow, hydropower generation, and downstream water resources (NCHM, 2018). The National Centre for Hydrology and Meteorology (NCHM) has designated Gangju La, Thana, and Shodug glaciers as benchmark glaciers for long-term glacier monitoring. Previous in situ observations from Bhutan have shown persistent negative mass balance, with stronger melt generally observed at lower elevations (Tshering & Fujita, 2016). Since Bhutanese glaciers are influenced by both the Indian Summer Monsoon and winter westerly systems, annual mass-balance measurements alone may not fully capture the seasonal processes controlling glacier gain and loss. The timing and seasonality of precipitation are especially important for summer-accumulation glaciers, where accumulation and ablation may occur during the same season (Fujita, 2008).

Shodug Glacier, located at the headwaters of Thim Chhu, has been monitored annually by NCHM since 2022 and has become an important site for both annual and seasonal glacier mass-balance observation.

Previous reports documented continued glacier mass loss and terminus recession during 2022–2024 and 2024–2025, establishing the baseline for long-term monitoring (NCHM, 2024;

NCHM, 2025a). The 2022–2024 report documented an annualized geodetic mass balance of −1897.60 ± 295.11 mm w.e. a^{-1} and a mean terminus recession of 48.62 m. The 2024–2025 report documented a geodetic mass balance of −2791.08 mm w.e. a^{-1} and a direct mass balance of −2608.49 mm w.e. a^{-1}, together with a mean terminus recession of 15.07 m.

In 2025, seasonal mass-balance monitoring was initiated jointly by NCHM and ICIMOD. The first seasonal assessment covered May–November 2025 and reported a cumulative geodetic mass balance of −1876.70 mm w.e. (NCHM & ICIMOD, 2025). This assessment established the first seasonal component of the 2025–2026 annual monitoring cycle and provided the methodological basis for examining the complementary November 2025–May 2026 winter-season balance.

The present report continues this monitoring history by estimating the annual geodetic mass balance of Shodug Glacier for May 2025–May 2026 and the winter-season mass balance for November 2025–May 2026. The annual analysis is based on repeat RTK GNSS surface-elevation measurements, elevation-change modelling, 50 m elevation-band integration and glacier hypsometry. The winter-season balance is also evaluated using repeat geodetic measurements and snow-depth observations. Sawdust markers installed on the November 2025 snow surface are analysed separately as reference horizons for interpreting snowpack evolution and are not used directly in the mass-balance calculation.

2 Aim and Objectives

The primary aim of this study is to assess the annual and seasonal mass balance of Shodug Glacier for the 2025–2026 monitoring period using field-based geodetic observations, thereby contributing to Bhutan’s long-term benchmark glacier monitoring programme.

The specific objectives of this study are to:

1. install new stake for the glaciological year 2026-2027
2. estimate the annual glacier-wide mass balance of Shodug Glacier for May 2025–May 2026 using the in situ geodetic method;

3. estimate the winter-season mass balance for November 2025–May 2026 using in situ geodetic method, and document marker-referenced winter snow-surface changes using the sawdust horizons;

4. assess the spatial pattern of surface elevation change and mass balance across 50 m elevation bands;

5. map and quantify terminus recession during the 2025–2026 monitoring period;

6. provide a continued scientific basis for long-term glacier monitoring, water-resource assessment, and climate-change impact studies in Bhutan.

7. quantify and propagate uncertainties geodetic estimates.

3 Study Area

3.1 Location

Shodug Glacier is a clean-ice cirque glacier located in the headwaters of the Thim Chhu river system in Bhutan. Its current mapped area is approximately 1.110 km². The glacier lies within WGS 84/UTM Zone 45N, approximately at 27.940° N and 89.950° E. It extends from about 5,100 to 5,500 m a.s.l. The glacier is important from both cryospheric and hydrological perspectives, as its meltwater contributes to the flow of Thim Chhu and supports downstream water availability.

3.2 Accessibility

Shodug Glacier is accessed through the Thimphu–Barshong–Shodug route. The approach to the field site generally requires about three days of walking from the road head, depending on weather, trail condition, and field logistics. The base camp is located at Pam Luma, at approximately 4,900 m a.s.l. From the base camp, the glacier can be reached in about two hours on foot.

3.3 Glacier Monitoring Setup on Shodug Glacier

The monitoring setup on Shodug Glacier includes repeated dGPS surface-elevation surveys, terminus mapping, glacier-stake observations. A fixed dGPS base station point has been used during field surveys to support repeated high-precision surface-elevation measurements. In May 2025, seven bamboo stakes were installed along the glacier centreline, covering the elevation gradient from the upper glacier to the lower ablation area. An automatic weather station was also installed on the glacier to support meteorological observation for future glacier-climate studies. For the year 2026-2027, the team installed seven bamboo ablation stakes spanning the glacier's elevation gradient from the accumulation zone at the head to the lower ablation zone to capture the known dependency of melt on elevation (Tshering & Fujita, 2016) along the centreline of the glacier.

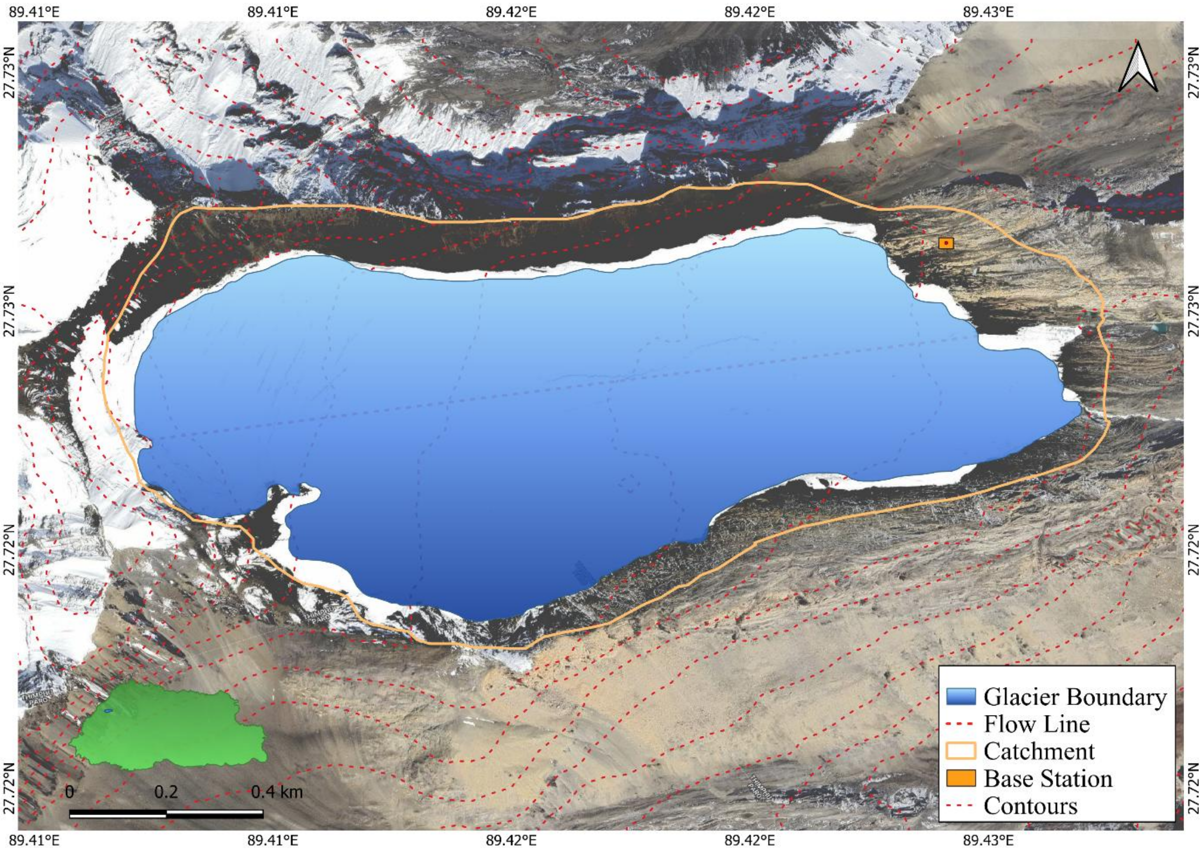

Figure 1. Shodug Glacier

4 Data and Methodology

4.1 Data Acquisition

Field data for this study were collected during the May 2025, November 2025, and May 2026 field campaigns on Shodug Glacier. The field observations included dGPS surface-elevation surveys, snow-depth measurements, snow-stake readings, sawdust-marker measurements, terminus mapping, and replacement stake installation. The dGPS data provided the basis for geodetic surface-elevation change. Sawdust-marker measurements were analysed independently as evidence of relative movement of the marked November snow horizon and were not included in the mass-balance equation.

The glacier surface-elevation survey was carried out using a calibrated Trimble R10-2 RTK GNSS system. The base station was established on the previously marked reference point located outside the glacier surface. The known coordinates of the base station were entered into the TSC7 controller, and the antenna height was measured and recorded before starting the survey. The rover was mounted on a backpack, and glacier surface points were collected by walking across the glacier, following the previous survey tracks as far as field conditions allowed. Data were recorded in continuous topo mode with close point spacing. Additional points were collected where necessary to improve spatial coverage, especially in areas where snow condition, surface exposure, or access differed from previous surveys. The same general survey approach was used for both annual and seasonal observation periods.

During the November 2025 field campaign, the glacier surface was fully covered by snow brought by Cyclonic Storm Montha from 26 October to 1 November 2025. As a result, five glacier stakes towards the accumulation zone were fully submerged under snow. To assess the effect of this unusual snow cover and to support seasonal monitoring, snow stakes were installed in close proximity to the glacier-stake locations. At each snow-stake site, snow depth was measured within a 1 m × 1 m square sampling plot. Nine snow-depth measurements were taken within each plot: one at each corner, one at the midpoint of each side, and one at the centre. All measurements were obtained by inserting a probe vertically into the snow layer until the underlying glacier ice surface was reached. The exposed length of each snow stake above the current snow surface was also measured and recorded (NCHM & ICIMOD, 2025).

A 50 cm × 50 cm sawdust layer was placed at each snow-stake site on the November 2025 snow surface to create a visible reference horizon for recovery during the May 2026 visit. It was intended to remain buried and was assumed to have negligible influence on the overlying winter snow; if marker material becomes exposed, however, it can disturb local melt, so marker recovery and snow-stake readings were treated independently. The area around each snow stake was excavated to the sawdust layer, and the distance from the fixed stake reference to the recovered marker horizon was measured.

Glacier terminus mapping was also carried out using the dGPS rover. The survey team walked along the visible glacier terminus and collected a profile of the current snout position. This terminus line was later compared with previously mapped terminus positions to estimate horizontal terminus recession. Since the terminus position changes from year to year, it was mapped independently from the fixed surface-elevation survey tracks.

During the May 2026 field visit, the glacier stakes installed in May 2025 could not be recovered because they were covered by snow. Therefore, direct annual mass balance based on continuous glacier-stake readings could not be calculated for the May 2025–May 2026 observation period. To maintain the long-term monitoring network, new replacement stakes were installed in close proximity to the previous stake locations using the available coordinates of the original stakes. These new stakes will serve as reference points for future direct/glaciological mass-balance measurements.

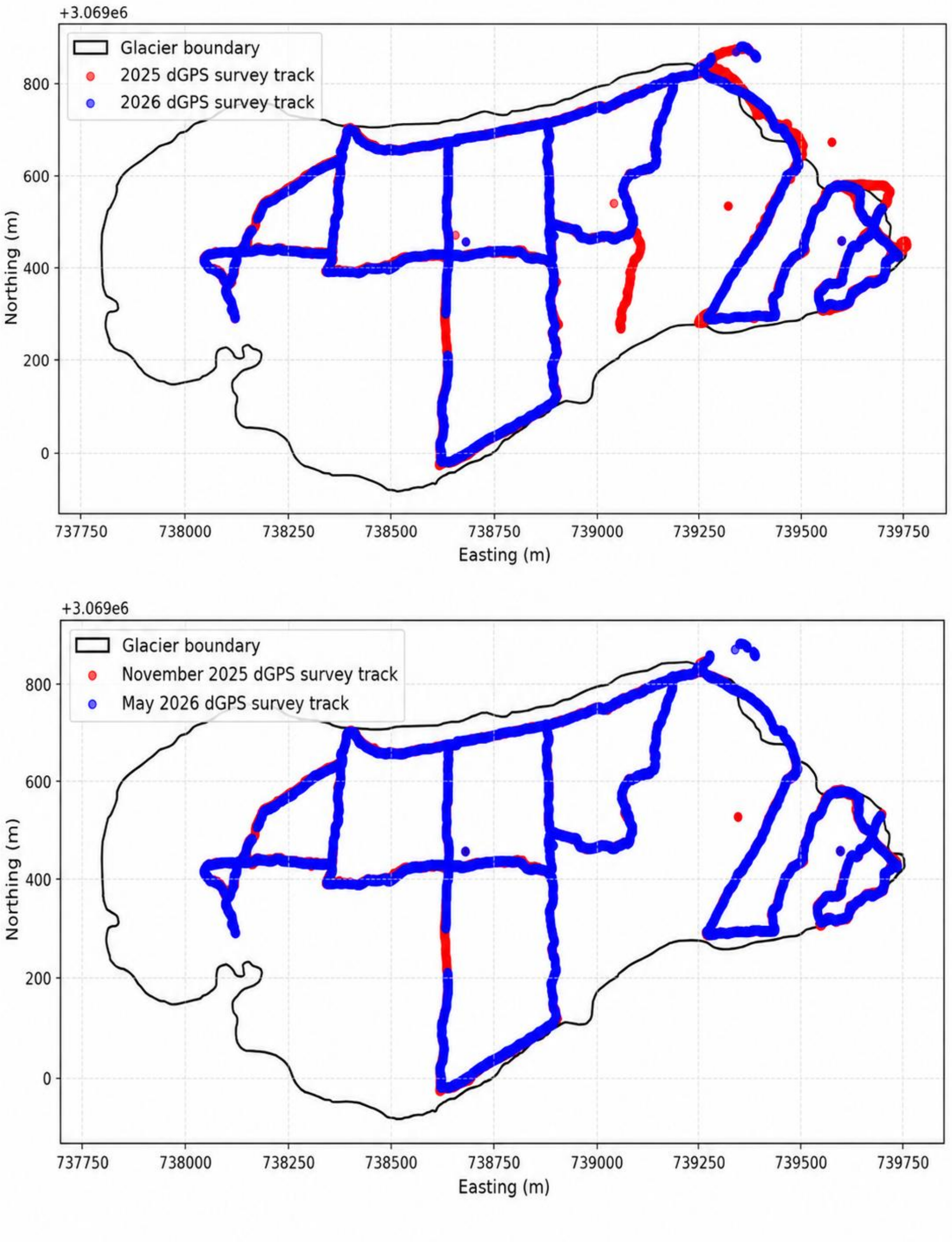

Figure 2. dGPS survey tracks for annual mass balance and seasonal mass balance

Figure 3. RTK GNSS base-station setup used during the field survey.

4.2 Data post-processing

4.2.1 Overview of approach, datasets, and inputs

Geodetic approach

For the geodetic mass-balance calculation, dGPS surface-elevation points from the earlier survey period (t1) and the later survey period (t2) were used as direct observations of the glacier surface at the time of each survey. These dGPS points were processed in a common coordinate reference system and used to calculate surface elevation change. The elevation changes derived from the dGPS surveys formed the main basis for estimating geodetic mass balance. This approach follows the standard definition of the geodetic method, where glacier mass balance is inferred from repeat mapping of glacier surface elevations and the resulting elevation or volume change is converted to water equivalent using appropriate density assumptions (Cogley et al., 2011; Kaser et al., 2003).

Glaciological or direct approach

n standard glacier mass-balance terminology, the direct method is synonymous with the glaciological method and refers to in situ measurements of accumulation and ablation on the glacier surface, generally using glacier ablation stakes, snow pits, snow-depth probing and density measurements at fixed or repeated measurement sites (Cogley et al., 2011; Kaser et al., 2003). These point measurements are then extrapolated or integrated across elevation bands to estimate glacier-wide mass balance.

For the May 2025–May 2026 observation period, the direct/glaciological method could not be applied because the glacier stakes installed in May 2025 were not recovered during the May 2026 field visit. Therefore, snow-stake and snow-depth observations in this report are not treated as substitutes for glacier-stake readings; they are used only to support snow-storage interpretation and the geodetic density-conversion term.

DEM raster and Glacier Outline

A DEM raster and glacier outline were used to support the spatial calculation of glacier-wide mass balance. Field-based dGPS glacier surface elevation points were then used for quality control and to apply a vertical bias correction to the 1 m DEM (Maxar). The corrected DEM, clipped to the mapped glacier extent using the glacier outline polygon, was subsequently used to derive glacier hypsometry (area distribution by elevation bands) and to ensure all terrain analyses were restricted to the glacier area.

Snow depth

Snow-depth measurements and stake elevations collected on two survey dates were used to estimate snow thickness at the midpoint of each 50 m elevation band.

Main input datasets

The main datasets used in the analysis are:

1. dGPS surface-elevation points from the earlier survey period;
2. dGPS surface-elevation points from the later survey period;
3. DEM raster;

4. glacier outline;

5. snow-depth data from the earlier and later survey periods.

Software and processing environment

Remote sensing data preparation and geospatial preprocessing were carried out using a combination of cloud-based and desktop GIS tools alongside Python. A Sentinel-2 median composite (2025; 10 m) was extracted using Google Earth Engine (GEE) to support glacier boundary identification. The glacier outline was then manually delineated in QGIS, which was also used for study area mapping. Subsequent data processing and analysis were implemented in Python using standard scientific and geospatial libraries. Numerical computation and tabular data handling were performed with NumPy and Pandas, while figures and plots were produced using Matplotlib. Vector geospatial operations (e.g., handling glacier outlines, point geometries, and spatial joins) were carried out using GeoPandas, with Shapely used for geometry construction and manipulation. Raster-based DEM processing, including reading and masking/clipping to the glacier boundary, was conducted using Rasterio (including rasterio.mask). Robust trend fitting for elevation-dependent modelling (e.g., Δh–elevation relationships) was implemented using TheilSenRegressor from scikit-learn.

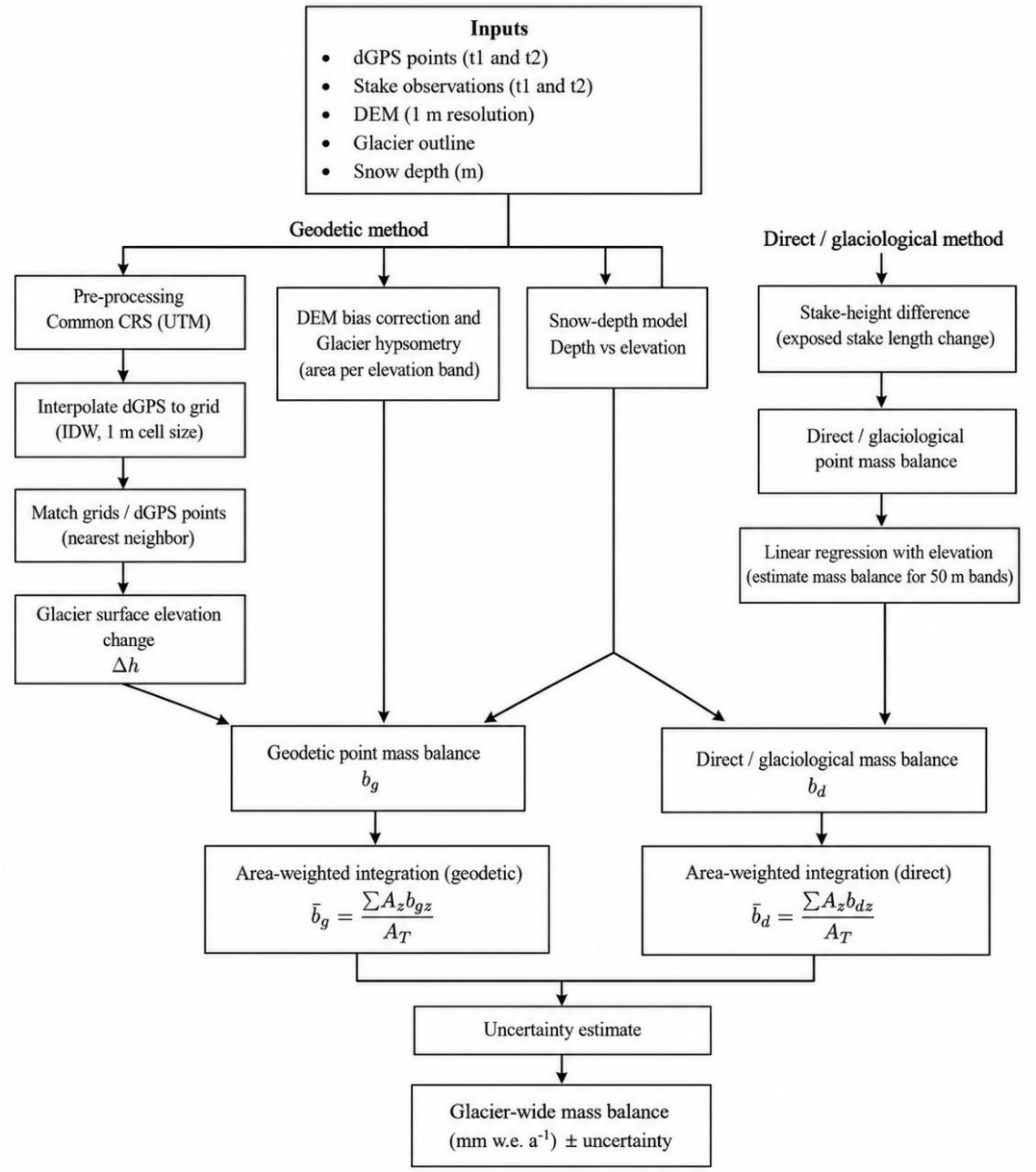

Figure 4. Workflow used for the Shodug Glacier mass-balance assessment.

4.2.2 Preprocessing and quality control

Annual and seasonal datasets were processed independently. The annual analysis paired the May 2025 and May 2026 surveys, while the seasonal analysis paired November 2025 and May 2026. All datasets were checked for required coordinate and elevation fields, non-numeric or missing values, exact duplicate records, coordinate ranges, elevation ranges and spatial overlap. The dGPS points, DEM and glacier outline were verified in WGS 84/UTM Zone 45N (EPSG:32645), with horizontal coordinates and elevations expressed in metres.

No missing or non-numeric coordinate or elevation records were identified. Exact duplicate dGPS records were detected in the May 2025 and May 2026 datasets and were flagged for removal before final processing to prevent repeated observations from disproportionately influencing the IDW interpolation. No exact duplicates were found in the November 2025 dataset. All three snow-depth datasets contained seven complete observations without missing or duplicate records.

Table 1. Summary of input-data quality control and retained matched-grid observations.

Analysis period	**Input dGPS records at t_1/t_2**	**Invalid records**	**Exact duplicates at t_1/t_2**	**Unique records at t_1/t_2**	**Matched grid points retained in elevation bands**	**Snow-depth sites at t_1/t_2**
Annual: May 2025–May 2026	20,944/11,614	0 / 0	13,081/2,554	7,863/9,060	7,685	7 / 7
Seasonal: November 2025–May 2026	6,909/11,614	0 / 0	0 / 2,554	6,909/9,060	8,539	7 / 7

The matched values represent co-located 1 m interpolated grid points retained within the 50 m elevation-band domain, rather than the original raw dGPS observations. Annual and seasonal outputs were stored separately to prevent observations from the two monitoring periods from being mixed during matching, elevation-band aggregation and glacier-wide integration. Bands without accepted matches were retained as missing and subsequently identified as modelled values where elevation-dependent extrapolation was required.

4.2.3 Interpolation of dGPS points onto a 1 m grid (IDW)

The dGPS observations followed repeat walking transects and were therefore irregularly spaced rather than arranged on a raster. For each survey date, the cleaned surface-elevation points were interpolated onto a regular 1 m grid using inverse distance weighting (IDW). The same cell size, search radius, and weighting power were used for the two annual surfaces and for the two seasonal surfaces. Only grid nodes with at least one contributing dGPS observation were exported, together with a point identifier, UTM easting, UTM northing, interpolated elevation, and a sorting field used for diagnostic plots. The gridding step standardised the spatial representation of each repeat survey while retaining the dense geometry of the measured tracks.

4.2.4 Grid definition and neighbourhood search

For each survey, the grid extent was defined from the minimum and maximum dGPS eastings and northings and was expanded by half a cell at each edge. Grid nodes were generated at 1 m spacing in UTM Zone 45N. A SciPy cKDTree was built from the measured dGPS coordinates, and a radius query identified all observations within 0.7 m of each grid node. Nodes without a neighbour inside this radius were assigned no-data and omitted from the exported point grid. Because the search radius was deliberately local, the interpolation was confined to the immediate vicinity of the measured transects rather than extrapolated across unsurveyed parts of the glacier.

4.2.5 IDW formulation and assumptions

IDW assumes that surface elevations measured close to a prediction location are more representative than measurements farther away. The elevation at a valid grid node was therefore calculated as a weighted mean of the neighbouring dGPS elevations found within the 0.7 m search radius.

For a grid node at location x, the interpolated elevation was calculated as:

$$\hat{z}(x) = \frac{\sum_{i=1}^{n} w_i z_i}{\sum_{i=1}^{n} w_i}, w_i = \frac{1}{d_i^p} \quad (1)$$

where z_i is the observed surface elevation at neighbour i, i is its planimetric distance from the grid node, and p is the IDW power. A power of p = 2 was used, giving inverse-distance-squared weighting. This choice gives the closest measurements the greatest influence while allowing nearby observations to reduce local measurement noise. If a measurement coincided with a grid node (d_i = 0), its measured elevation was assigned directly, so the interpolation remained exact at observation locations. The approach assumes metre-scale continuity of the glacier surface within the search neighbourhood and does not infer elevations where no nearby dGPS observation was available.

4.2.6 Co-location of survey periods and elevation change computation (Δh)

Elevation change was calculated separately for the annual and seasonal periods. For each period, the later gridded surface (t2) was used as the left-hand dataset in a nearest-neighbour spatial join with the earlier gridded surface (t1). Candidate neighbours were first searched within a broad maximum distance of 50 m to avoid unrestricted matches in sparse areas. The joined pairs were then restricted to a nearest-neighbour distance of 3 m or less. The accepted distance was retained as a quality-control attribute and inspected against elevation change to identify possible mismatches. This procedure was applied to the 2025–2026 annual pair and repeated, without mixing records, for the November 2025–May 2026 seasonal pair.

4.2.7 Elevation changes at matched points

For every accepted pair, surface-elevation change was calculated using the later surface minus the earlier surface:

$$\Delta h = h_{t2} - h_{t1} \quad (2)$$

where h_t2 and h_t1 are the co-located dGPS surface elevations at the later and earlier survey dates, respectively. Under this sign convention, positive Δh denotes surface rise or accumulation and negative Δh denotes surface lowering or ablation. The matched annual and seasonal Δh datasets were inspected independently using transect plots, Δh-versus-distance plots, elevation-change distributions, and Δh-versus-elevation plots before elevation-band aggregation.

4.2.8 DEM vertical bias check and correction

The reference Maxar DEM was used to derive elevation bands and glacier hypsometry. Before this use, DEM elevations were sampled at the corresponding dGPS coordinates and compared with the field elevations. The signed residual at each sampled location was calculated as:

$$\Delta z_{DEM-dGPS} = z_{DEM} - z_{dGPS} \tag{3}$$

The mean signed residual was used as a first-order estimate of the vertical offset. The offset was subtracted from the DEM to produce the corrected surface shown below:

$$z_{DEM,corr} = z_{DEM} - bias. \tag{4}$$

The raw and corrected residual distributions and elevation profiles were then inspected to confirm that the mean vertical offset had been removed and to identify any remaining elevation-dependent or spatial pattern. The same bias-check procedure was used for the annual and seasonal workflows. The corrected DEM was used only for the area-elevation distribution and band assignment; annual and seasonal Δh values themselves were obtained directly from the repeat dGPS surveys. Figure 5 compares the raw and corrected DEM profiles for both processing periods.

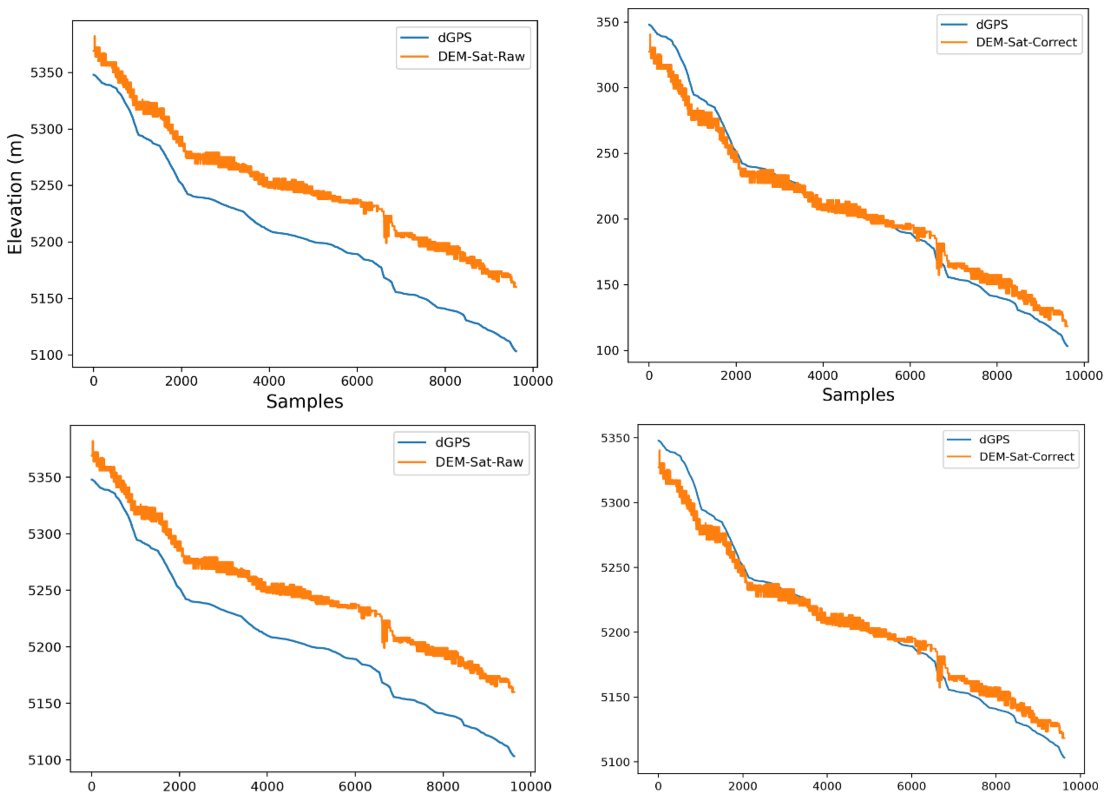

Figure 5. DEM vertical-bias diagnostics used in the annual and seasonal workflows. The upper panels show the annual comparison between dGPS and the raw and bias-corrected Maxar DEM; the lower panels show the corresponding seasonal comparison.

4.2.9 Glacier hypsometry (area–elevation distribution)

Glacier hypsometry describes the distribution of glacier area with elevation and provides the spatial weighting required to scale the surveyed transects to the whole glacier. The same 2026 glacier outline was used for both endpoint DEMs. For each workflow, the vertically corrected DEM was clipped to the mapped glacier outline. No-data and non-glacier pixels were excluded, and the remaining DEM cells were classified using common 50 m elevation-band edges. For elevation band z, the corresponding glacier area was calculated as:

$$A_z = N_z r^2 \tag{5}$$

where N_z is the number of valid DEM pixels in elevation band z and r is the DEM pixel size in metres; r^2 is therefore the area of one pixel. The same elevation-band definition was used for Δh, snow depth, and geodetic mass-balance integration.

Where the band areas associated with the two survey dates differed, the representative band area was taken as the mean of the two date-specific areas following Tshering and Fujita (2016):

$$A_z = \frac{A_{t1} + A_{t2}}{2} \tag{6}$$

where A_{t1} and A_{t2} are the glacier areas in the same 50 m band at the earlier and later survey dates. If a common outline was used for both dates, the same hypsometry was used directly. Annual and seasonal hypsometry were kept with their respective workflows and were checked against the polygon area to ensure that the sum of all band areas represented the mapped glacier extent. Figure 6 presents the area–elevation distributions used for the two analyses.

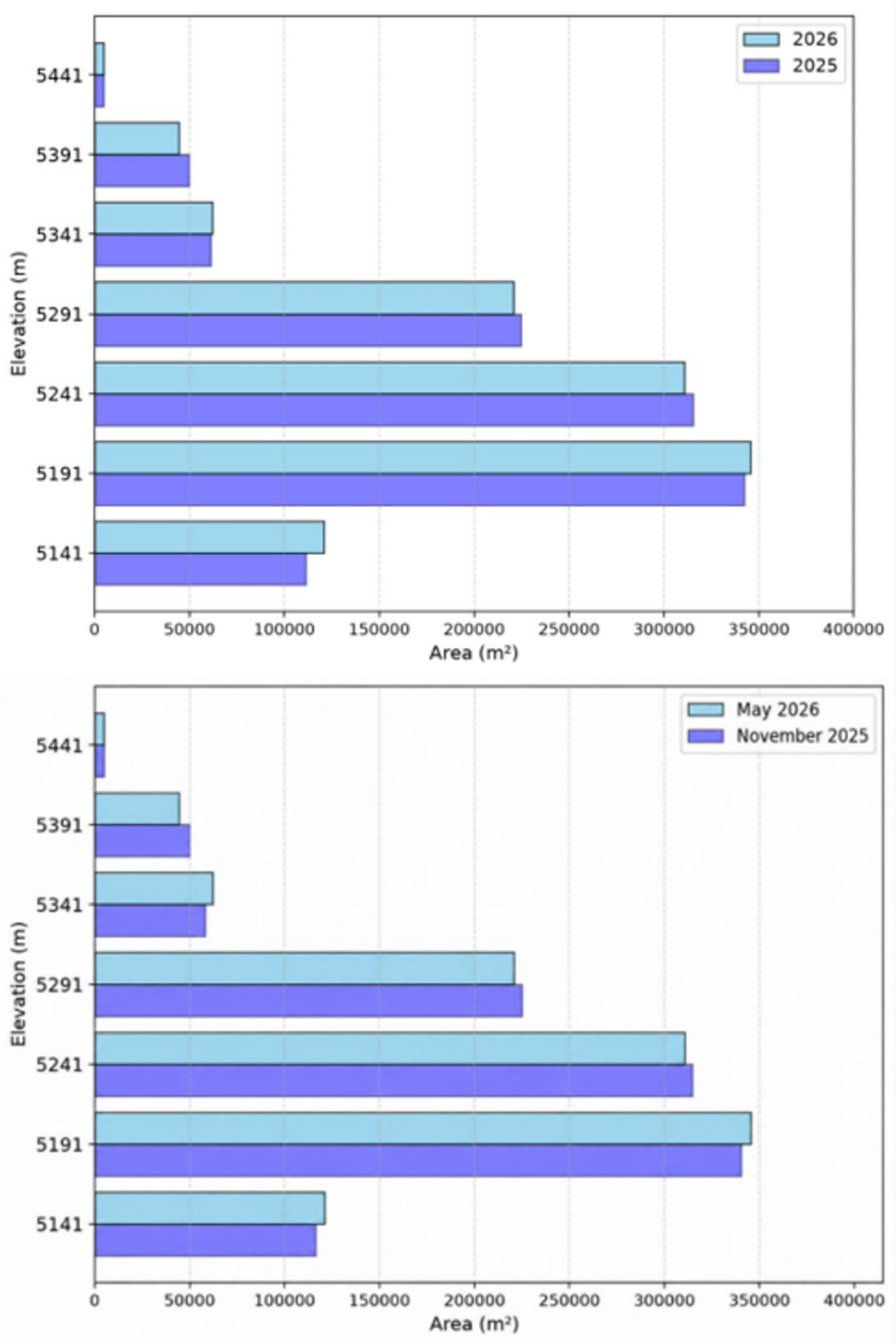

Figure 6. Glacier hypsometry used for area weighting in the annual analysis (upper panel) and the seasonal analysis (lower panel). Areas are summarized in 50 m elevation bands.

4.2.10 Elevation-band aggregation of Δh and robust smoothing

Accepted matched points were assigned to 50 m elevation bands using the elevation of the later survey. For each band, the number of matched points and arithmetic mean surface-elevation change (Δh) were calculated separately for the annual and seasonal periods.

A Theil–Sen regression was fitted between observed band-mean Δh and band-midpoint elevation. The primary series retained the observed mean in bands containing matched points and used the fitted value only for bands without observations. Therefore, values assigned to empty bands represent modelled extrapolations rather than measured surface changes.

Table 2. Elevation bands without matched dGPS observations.

Analysis	**Elevation band (m a.s.l.)**	**Matched points**	**Modelled Δh (m)) (m)**	**Value source**
Annual	5366–5416	0	−0.226	Theil–Sen extrapolation
Annual	5416–5466	0	+0.231	Theil–Sen extrapolation
Seasonal	5366–5416	0	−0.099	Theil–Sen extrapolation
Seasonal	5416–5466	0	−0.194	Theil–Sen extrapolation

Accordingly, the positive annual of Δh (m) of +0.231 m in the highest elevation band is an extrapolated estimate and should not be interpreted as an observed surface rise.

A fully fitted sensitivity series was also calculated by applying the Theil–Sen prediction to every elevation band, including bands with observations. For the annual May 2025–May 2026 period, the fully fitted estimate was −1733.87 mm w.e., compared with the primary hybrid estimate of −1769.48 mm w.e. For the November 2025–May 2026 seasonal period, the fully fitted estimate was +90.46 mm w.e., compared with the primary estimate of +80.60 mm w.e. The relatively small differences indicate that the glacier-wide results are not strongly dependent on the selected elevation-band fitting approach. Figure 7 shows the annual and seasonal elevation-change patterns and their robust trends.

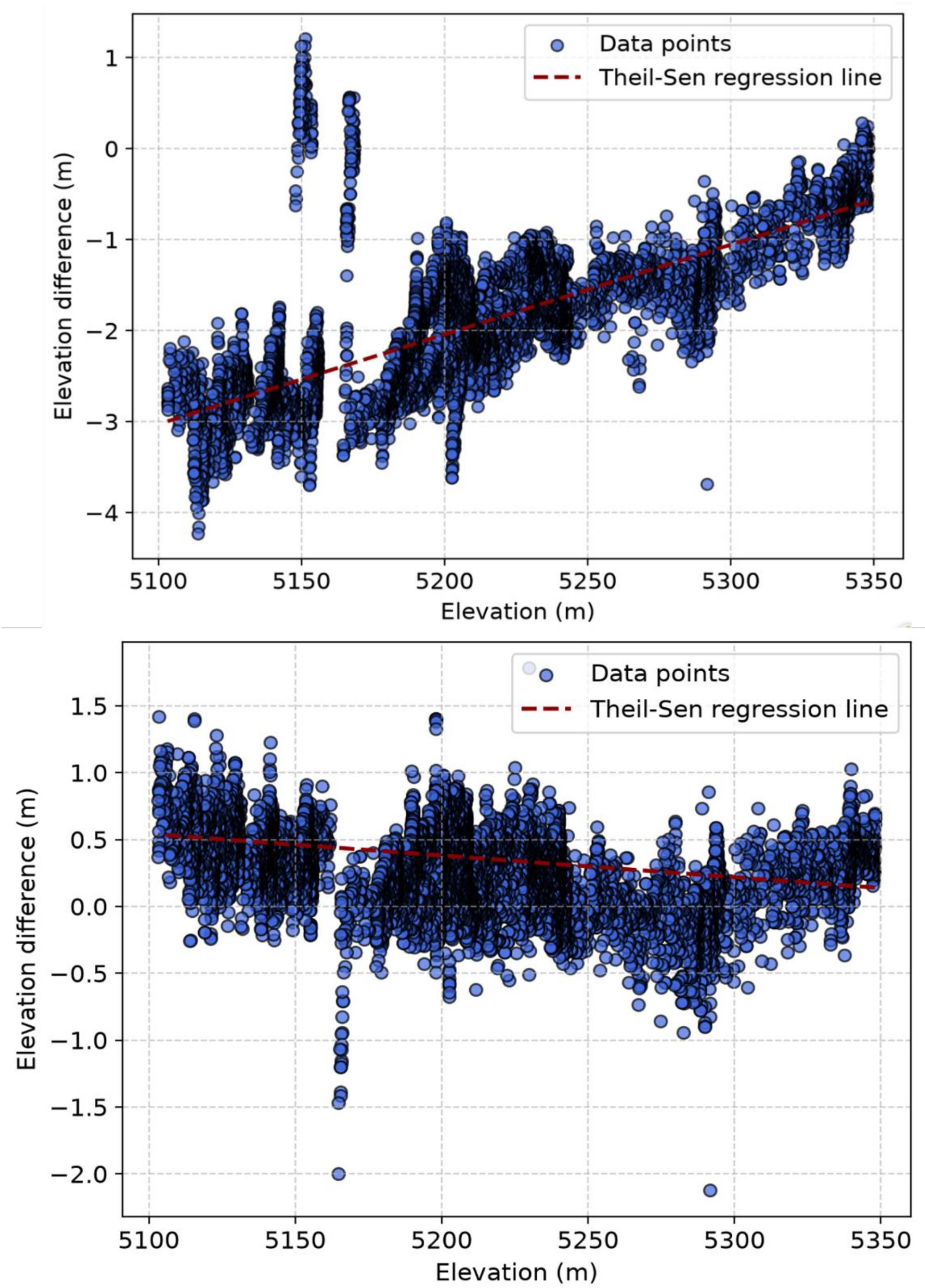

Figure 7. Surface-elevation change as a function of elevation with the fitted Theil–Sen trend for (upper) the annual 2025–2026 period and (lower) the seasonal November 2025–May 2026 period. Negative values indicate lowering and positive values indicate

4.2.11 Snow depth–elevation model and ΔS(z)

Snow depth change (ΔS) can be derived from stake measurements collected on two survey dates and parameterized as a function of elevation so that it can be applied consistently across the same 50 m elevation bands used for hypsometry and elevation-change integration. In such a case, stake observations consist of snow depth (m) and stake elevation (m), and the goal is to estimate representative snow depth at the midpoint of each 50 m elevation band. Annual snow-storage change used the snow observations associated with the two annual endpoints, while seasonal snow-storage change used the November 2025 and May 2026 snow measurements. Stake identifiers and elevations were checked to maintain correspondence between dates. Because only seven stake sites are available, fitted values, residuals, and the influence of individual stakes were examined and the model uncertainty was carried forward. Band-wise snow-depth change was calculated as:

$$\Delta S(z) = S_{t2}(z) - S_{t1}(z) \qquad (7)$$

4.2.12 Conversion to mass balance (point-wise and area-averaged)

The same density-conversion framework was applied to the annual and seasonal elevation-change series. Repeat dGPS surveys measure change in the snow-covered glacier surface. Consequently, treating the entire Δh as ice would be inappropriate where endpoint snow depths differ. The snow-depth term ΔS(z) was therefore used to separate the density effect of the changing snow layer from the ice-equivalent component. Calculations were performed for each 50 m elevation band and were then integrated with the period-specific glacier hypsometry.

Band-wise geodetic mass balance

For elevation band z, the mass change per unit area over the observation interval was calculated as:

$$b_{gz} = \frac{\Delta h_g(z)\,\rho_i + \left(s_{t2}(z) - s_{t1}(z)\right)(\rho_s - \rho_i)}{t_2 - t_1} \qquad (8)$$

where $\Delta h_g(z)$ is the annual or seasonal band-mean surface-elevation change, ΔS(z) $\left(s_{t2}(z) - s_{t1}(z)\right)$, ρ_i is ice density, and ρ_s is snow density. Values of ρ_i= 880 kg m^{-3} and ρ_s= 400 kg m^{-3} were used in the implemented workflow. The expression yields kg m^{-2}, which is numerically equivalent to mm water equivalent (mm w.e.). Division by water density (ρ_w = 1000 kg m^{-3}) gives metres water equivalent. A rate in mm w.e. a^{-1} is reported only after division by the exact survey interval expressed in years.

Glacier-wide area-averaged mass balance

The glacier-wide specific balance was obtained by weighting each band value by its representative glacier area:

$$\underline{b_g} = \frac{\sum_z A_z \, b_{gz}}{A_T} \tag{9}$$

where A_z is the representative area in elevation band z and $A_T = \Sigma A_z$ is the total glacier area. The annual band balances and annual hypsometry were integrated to obtain the annual geodetic balance; the seasonal band balances and seasonal hypsometry were integrated independently to obtain the November–May seasonal balance. This separation preserves the observation interval and prevents seasonal accumulation from being combined implicitly with the annual result.

4.2.13 Sawdust-marker observations of winter snow storage

In November 2025, sawdust markers were placed on the existing snow surface at eight sites to establish identifiable reference horizons. Artificial horizons such as sawdust have previously been used in glacier mass-balance programmes to facilitate the later identification of a known snow or firn surface beneath subsequent accumulation (O'Neel et al., 2019).

During May 2026, the buried markers were recovered by excavation, and the distance from each November marker horizon to the May snow surface was measured:

$$H_{winter,i} = z_{surface,May,i} - z_{marker,November,i}$$

This represents the net snow thickness retained above the November surface. Stake 3A was included only in the eight-site marker analysis and not in the seven-site direct mass-balance regression. Snow density was not measured; therefore, any water-equivalent conversion uses the assumed density of 400 kg m^{-3}.

Table 3. Saw-dust marker reading between November 2025 and May 2026

Site	November exposed stake reference (m)	May surface-to-marker snow thickness (m)
Stake 1	0.60	0.87
Stake 2	0.63	1.10
Stake 3	0.60	1.12
Stake 3A	0.84	1.17
Stake 4	0.82	1.16
Stake 5	0.70	1.01
Stake 6	0.67	1.08
Stake 7	0.89	1.16

4.2.14 Terminus mapping

During the field survey, the glacier terminus was mapped using dGPS by walking along the ice–land boundary at the glacier snout to record a continuous terminus line for the survey year. Terminus retreat was then calculated along the glacier flow direction by measuring the displacement between the current-year terminus and the reference terminus at multiple locations distributed across the snout. These measurements were taken along several flow-parallel segments, and the resulting retreat distances were averaged to obtain the mean terminus recession for that year.

5 Uncertainty Assessment

5.1 Area-averaged mass balance uncertainty

The area-average mass balance estimation is associated with three main uncertainties:

1. Uncertainty in the mass balance at each altitudinal band (db_Z; mm w.e. a^{-1}) is calculated for the bands.

2. Uncertainty from the glacier boundary delineation (dA_Z; m^2), and

3. Uncertainty from the assumed density of ice and snow (db_ρ; mm w.e. a^{-1}).

Because seasonal snow was present and ΔS(z) was included, both ice and snow density uncertainties were propagated in the uncertainty analysis. In the workflow, density uncertainties of ±30 kg m^{-3} for ice and ±100 kg m^{-3} for snow were applied, and the overall density-related uncertainty was computed from the combined ice and snow contributions (reported as Total Uncertainty Ice, Total Uncertainty Snow, and their average). The combined uncertainty (σ) is calculated following the methodology described in Tshering and Fujita (2016) as:

$$\sigma = \frac{\sum A_Z db_Z + \sum dA_Z |b_Z| + \sum A_Z db_\rho}{A_T} \quad (14)$$

Where:
- A_Z is the area within a 50 m altitudinal band,
-$A_T$is the total glacier area,
- b_Z is the mass balance at each band, and
- $|b_Z|$ is the absolute mass balance.

The uncertainty from the boundary delineation (dA_Z) is computed as:

dA_Z = 0.5 × pixel resolution × perimeter at each 50 m band

Given the Sentinel-2 MSI image resolution of 10 m, dA_Z is based on half the pixel size (i.e., 5 m) multiplied by the perimeter of the glacier outline at each altitudinal band (Fig. 9b).

The uncertainty from the density assumption, db_ρ, arises from variability in the assumed densities of ice and snow. These uncertainties are averaged to represent the overall density-related uncertainty in mass balance estimation. For more details on the rationale behind the uncertainty calculation and the densities assumed, refer to Annex D.

The standard deviation (db_Z) of the mass balance across altitudinal bands, representing the uncertainty from spatial mass balance variation, is calculated as:

$$db_Z = \sqrt{\frac{1}{N}\sum(b_Z - \underline{b_z})^2} \tag{15}$$

Where N is the number of elevation bands and $\underline{b_z}$ is the mean mass balance.

6 Results and Discussion

6.1 Area-averaged mass balance and uncertainty

The area-averaged annual mass balance of Shodug Glacier for May 2025–May 2026 was estimated at −1769.48 ± 306.329 mm w.e. a^{-1}, indicating substantial net mass loss. The November 2025–May 2026 seasonal geodetic mass balance was +80.60 ± 82.67 mm w.e. The reported uncertainty reflects the combined influence of elevation-band variability, glacier boundary delineation, and density assumptions used in the geodetic conversion (Annex A, Table A1), and provides an uncertainty-bounded estimate of recent glacier mass change under prevailing climatic conditions. Table 5 shows the cumulative glacier mass balance since 2023. It is important to note that the 2022-2024 value was annualized and applied to two annual intervals.

Table 4. Cumulative glacier mass balance.

No.	**Year**	**Annual GMB (mm w.e.)**	**Cumulative GMB (mm w.e.)**
1	2023	-1897.6	-1897.6
2	2024	-1897.6	-3795.2
2	2025	- 2791.08	-6586.28
3	2026	-1769.48	**-8,355.76**

Snowfall associated with Cyclonic Storm Montha may have contributed to the less-negative 2025–2026 annual balance by increasing end-of-ablation-season snow storage. However, the available observations do not permit formal attribution of the interannual mass-balance difference to this event alone.

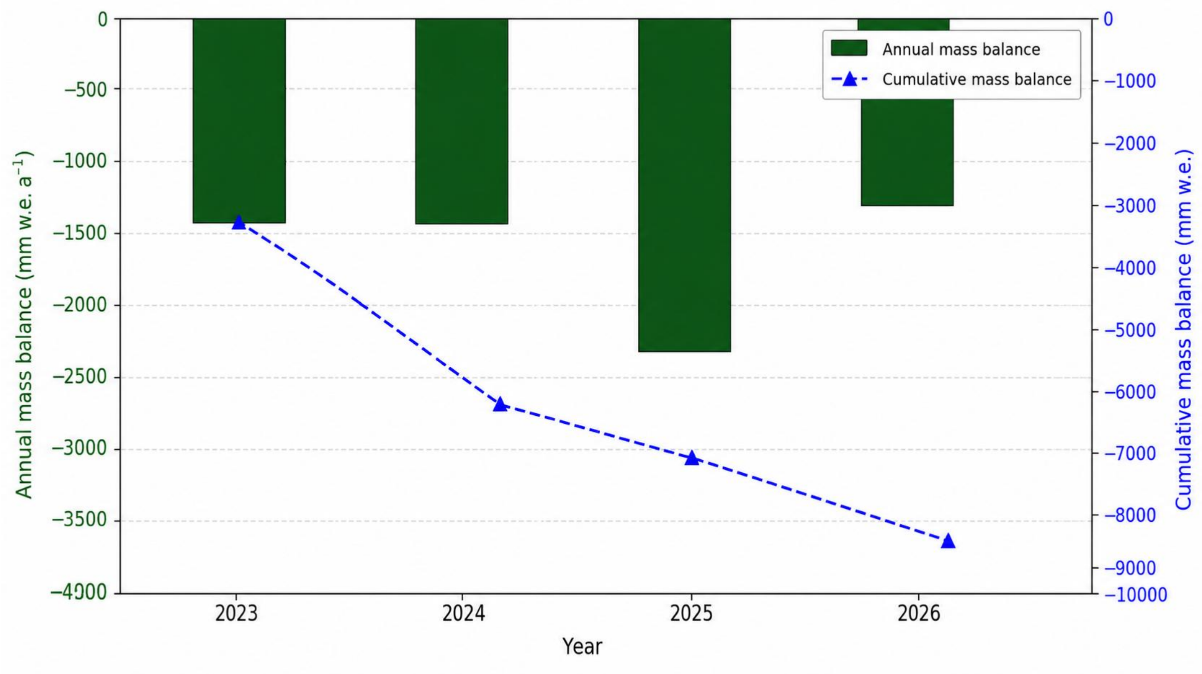

Figure 8. Annual and cumulative glacier mass balance over the monitored periods.

6.2 Seasonal mass-balance continuity and annual closure

The seasonal monitoring initiated jointly by NCHM and ICIMOD provides an opportunity to examine the contribution of the summer/monsoon and winter periods to the annual mass balance of Shodug Glacier. The previous seasonal assessment reported a cumulative geodetic mass balance of −1876.70 mm w.e. for May–November 2025. The present assessment estimated a cumulative geodetic mass balance of +80.60 mm w.e. for November 2025–May 2026.

Combining the two consecutive seasonal periods gives:

$$B_{seasonal\ sum} = B_{May-November} + B_{November-May}$$

$$B_{seasonal\ sum} = -1876.70+80.60 = -1796.10 = -1876.70 \text{ mm w.e. a}^{-1}$$

The independently calculated geodetic mass balance for the complete May 2025–May 2026 annual period was −1769.48 mm w.e. The closure residual between the annual estimate and the sum of the two seasonal estimates was therefore:

$$R = B_{annual} - B_{seasonal\ sum}$$

$$R = -1769.48-(-1796.10) = +26.62 \text{ mm w.e.}$$

The closure residual represents approximately 1.5% of the magnitude of the annual balance. This close agreement indicates good overall consistency between the independently processed annual and seasonal geodetic estimates. However, the residual should not be interpreted solely as measurement error because differences may also arise from survey-date offsets, spatial coverage, point matching, glacier hypsometry, snow-depth modelling, assumed densities and interpolation procedures.

6.3 Elevation-dependent surface lowering and hypsometric control

The annual elevation-difference distribution shows a mean Δh of -1.88 m, indicating widespread glacier surface lowering between May 2025 and May 2026. In contrast, the November 2025–May 2026 seasonal distribution shows a mean Δh of +0.27 m, indicating a net increase in glacier surface height during the winter/cold-season period. This positive seasonal Δh reflects snow accumulation over the glacier surface and is consistent with the positive seasonal geodetic mass balance of 80.60 mm w.e. However, the seasonal gain was not sufficient to offset the stronger annual-scale surface lowering, resulting in a negative annual mass balance of -1769.48 mm w.e. a^{-1}.

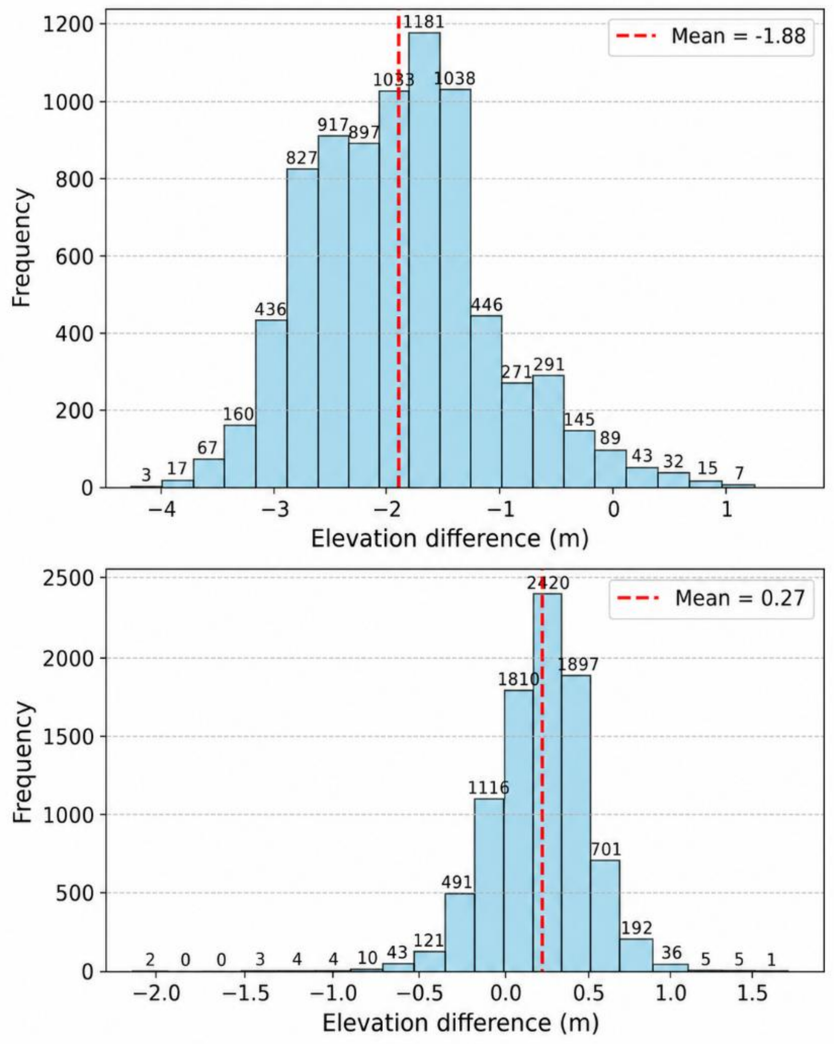

Figure 9. Distribution of glacier surface-elevation change during the annual 2025–2026 period (upper panel) and the seasonal November 2025–May 2026 period (lower panel).

Elevation-band analysis further refines the elevation-difference signal for Shodug Glacier. For the annual period, thinning was strongest in the lower elevation bands and generally decreased toward higher elevations. The lowest band (5,116–5,166 m a.s.l.) recorded a mean Δh of −2.509 m, while the uppermost band (5,416–5,466 m a.s.l.) showed a slight positive Δh of 0.231 m. The glacier-wide annual mass balance was −1769.48 mm w.e. a^{-1}. The largest contribution to this negative balance came from the 5,166–5,216 m band (−649.00 mm w.e. a^{-1}), mainly because this band contains the largest glacier area, about 31% of the total area. This shows that the annual mass-balance signal is controlled not only by the magnitude of thinning, but also by the glacier hypsometry.

For the seasonal period, the elevation-band results show a weaker and more mixed signal. The lower and middle elevation bands generally showed positive elevation change, with the lowest band (5,116–5,166 m a.s.l.) recording a mean Δh of 0.387 m. In contrast, some upper bands showed slight negative changes, with the highest band (5,416–5,466 m a.s.l.) recording −0.194 m. When integrated across the glacier area, the seasonal mass balance was slightly positive at 80.60 mm w.e. The largest positive contribution came from the 5,166–5,216 m band (38.53 mm w.e.), again reflecting the importance of glacier hypsometry in controlling the glacier-wide mass-balance signal.

6.4 Glacier area change

Using the 2026 Sentinel-2 median composite with 10 m spatial resolution, the Shodug Glacier boundary was manually digitized in QGIS. The mapped planimetric extent of the glacier for the 2025–2026 assessment was 1.11 km², equivalent to 1,110,155 m². This glacier outline was used to clip the vertically corrected DEM and to derive glacier hypsometry in 50 m elevation bands for area-weighted mass-balance integration.

The hypsometric analysis shows that the glacier area is mainly concentrated in the mid-elevation zone. The 5,166–5,216 m a.s.l. band contains the largest share of the glacier area, accounting for about 31% of the total glacier area, while progressively smaller areas occur toward the upper elevation bands. This distribution is important because the glacier-wide mass-balance signal is influenced not only by the magnitude of thinning but also by the area contained within each elevation band.

In previous assessments, the glacier area used for mass-balance calculation was approximately 1.22 km² for 2022–2024 and 1.16 km² for 2024–2025. In the present 2025–2026 assessment, the mapped area is 1.11 km². This indicates a continued reduction in mapped glacier area; however, a robust estimate of planimetric area change requires that year-specific outlines be delineated consistently from comparable imagery and supported by field-based terminus mapping.

6.5 Mass-balance gradient and ELA interpretation (2025–2026)

The annual mass-balance gradient was estimated using the five elevation bands containing matched dGPS observations. A linear regression was fitted between band-midpoint elevation and the corresponding primary annual point mass balance:

$$b(z) = 8.463z - 46081.17$$

where $b(z)$ is mass balance in mm w.e. and z is elevation in metres. The fitted relationship produced a mass-balance gradient of approximately +846 mm w.e. per 100 m elevation gain, with R^2=0.967 and an RMSE of approximately 111 mm w.e.

The zero crossing of the fitted relationship occurred at approximately 5,445 m a.s.l., representing the mass-balance-derived apparent equilibrium-line altitude for May 2025–May 2026. However, all bands containing matched dGPS observations had negative annual balances, and the highest observed band midpoint was 5,341 m a.s.l. The estimated ELA is therefore extrapolated approximately 104 m above the highest observed band midpoint and is not directly observed.

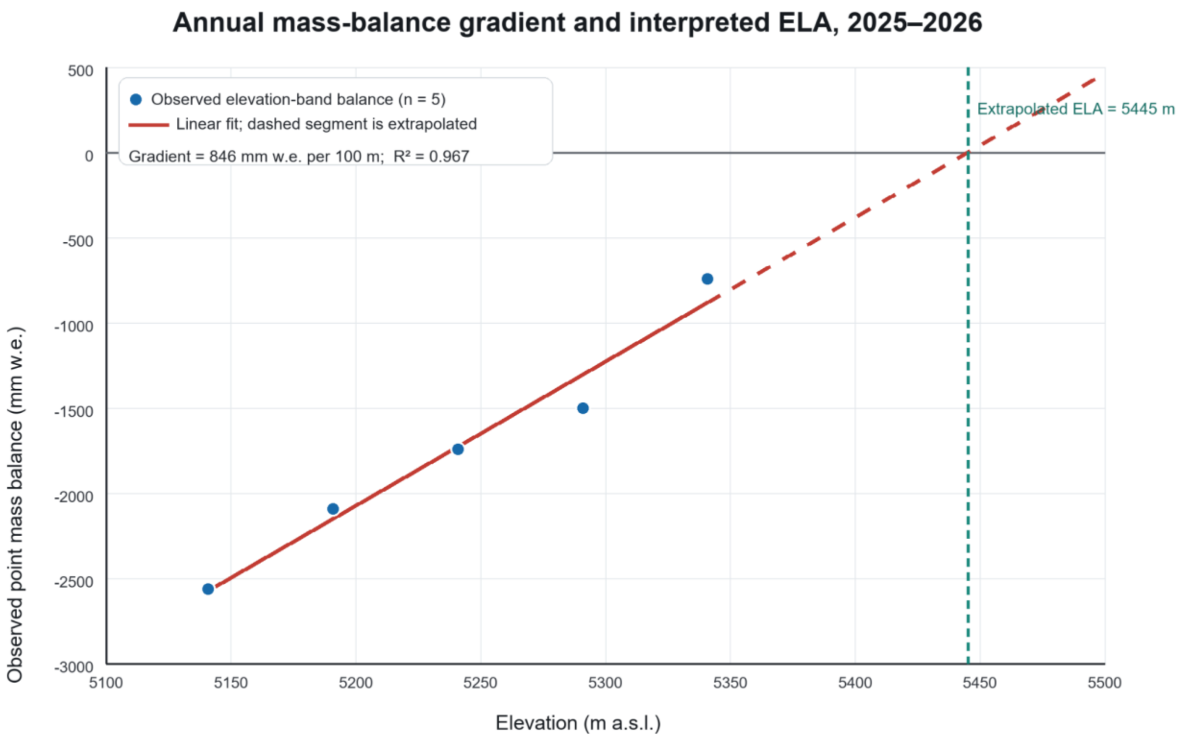

Figure 10. Relationship between elevation and primary annual point mass balance for the five elevation bands containing matched dGPS observations. The solid line represents the fitted relationship across the observed elevation range, while the dashed s

6.6 Winter snow storage from sawdust markers

All eight sawdust markers remained buried in May 2026. Surface-to-marker snow thickness ranged from 0.87 to 1.17 m, with a mean of 1.08 m and a median of 1.11 m. Using an assumed snow density of 400 kg m^{-3}, the unweighted mean retained snow storage was approximately

434 mm w.e., with site estimates ranging from 348 to 468 mm w.e.

The results provide independent evidence of positive winter snow storage and are consistent in sign with the positive seasonal geodetic balance. However, the marker measurements cannot separate gross snowfall from melt, compaction, or redistribution and should be treated as supplementary point observations rather than a glacier-wide mass-balance estimate.

6.7 Cumulative terminus recession

Mapping of the Shodug Glacier terminus between 2022 and 2026 indicates a clear pattern of frontal retreat. Terminus change was quantified using multiple transects drawn approximately orthogonal to the glacier front, allowing spatial variation in retreat distance to be assessed along different sectors of the terminus.

During the 2022–2024 period, the measured terminus recession ranged from 23.77 m to 70.45 m, with a mean retreat of approximately 48.62 m. Between 2024 and 2025, the terminus continued to recede, with a mean retreat of 15.07 m. For the 2025–2026 annual monitoring period, measured retreat distances ranged from 3.20 m to 27.20 m, with a mean retreat of 12.55 m. Although the magnitude of retreat during 2025–2026 was lower than the earlier 2022–2024 cumulative retreat, the terminus continued to show a consistent retreat signal.

The cumulative terminus recession of Shodug Glacier from 2022 to 2026 was estimated at 76.24 m. This persistent frontal retreat provides geometric evidence of continued glacier shrinkage and is consistent with the negative annual mass-balance conditions observed during the monitoring period.

Spatial differences in retreat distance along the glacier front are expected because terminus recession is influenced not only by glacier-wide mass balance, but also by local terminus geometry, surface slope, snow and debris cover, meltwater routing, and uneven downwasting. Therefore, the measured retreat should be interpreted as an integrated response of the glacier terminus to both local surface conditions and the broader negative mass-balance regime.

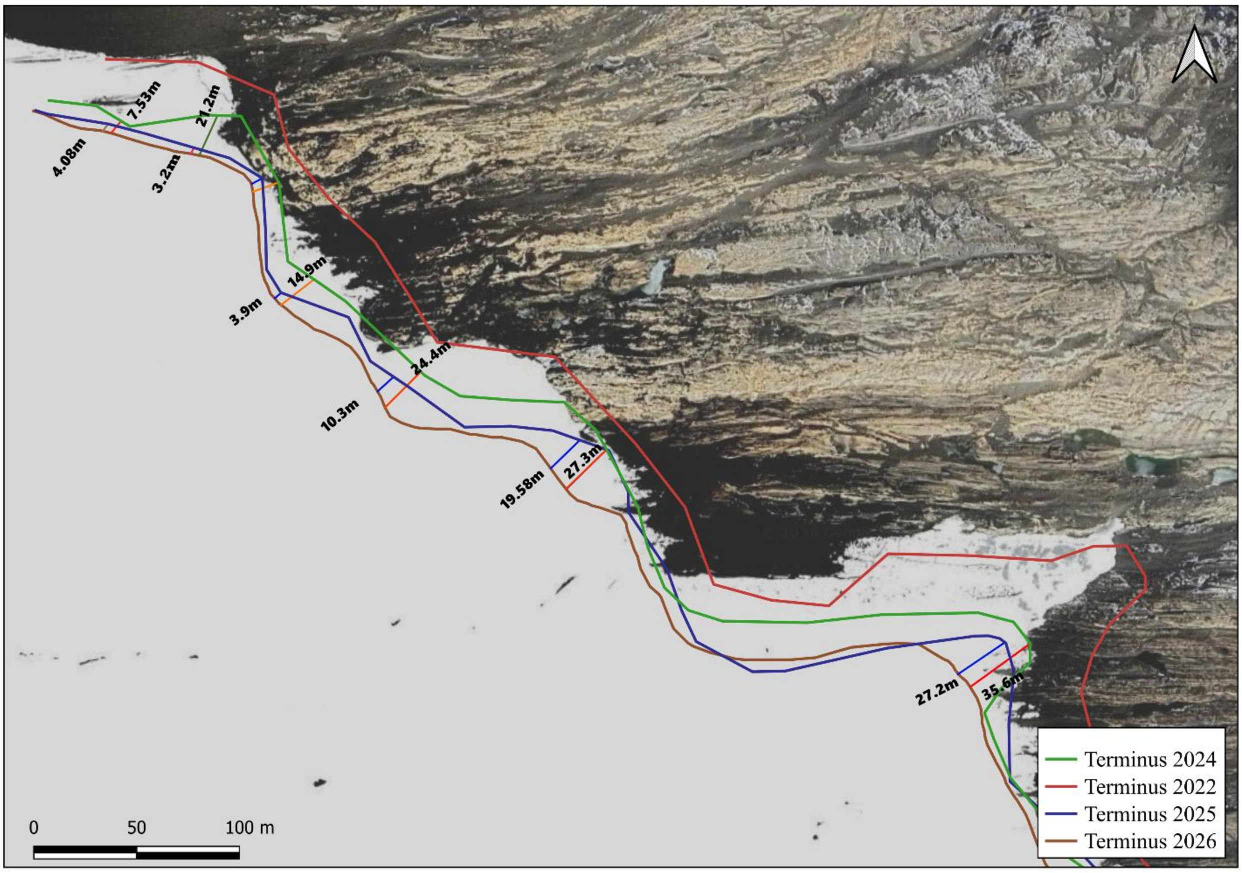

Figure 11. Cumulative terminus positions of Shodug Glacier from 2022 to 2026.

7 References

Azam, M. F., Wagnon, P., Berthier, E., Vincent, C., Fujita, K., & Kargel, J. S. (2018). Review of the status and mass changes of Himalayan-Karakoram glaciers. *Journal of Glaciology, 64*(243), 61–74. https://doi.org/10.1017/jog.2017.86

Cogley, J. G., Hock, R., Rasmussen, L. A., Arendt, A. A., Bauder, A., Braithwaite, R. J., Jansson, P., Kaser, G., Möller, M., Nicholson, L., & Zemp, M. (2011). *Glossary of glacier mass balance and related terms* (UNESCO-IHP Technical Documents in Hydrology No. 86). UNESCO International Hydrological Programme. https://wgms.ch/downloads/Cogley_etal_2011.pdf

Fujita, K. (2008). Influence of precipitation seasonality on glacier mass balance and its sensitivity to climate change. *Annals of Glaciology, 48*, 88–92. https://doi.org/10.3189/172756408784700824

Hugonnet, R., McNabb, R., Berthier, E., Menounos, B., Nuth, C., Girod, L., Farinotti, D., Huss, M., Dussaillant, I., Brun, F., & Kääb, A. (2021). Accelerated global glacier mass loss in the early twenty-first century. *Nature, 592*, 726–731. https://doi.org/10.1038/s41586-021-03436-z

Kaser, G., Fountain, A. G., & Jansson, P. (2003). *A manual for monitoring the mass balance of mountain glaciers* (UNESCO-IHP Technical Documents in Hydrology No. 59). UNESCO International Hydrological Programme. https://wgms.ch/downloads/Kaser_etal_UNESCO_2003.pdf

NCHM. (2018). *Bhutan glacier inventory 2018*.

NCHM. (2024). *Spring mass balance on Shodug Glacier, 2022–2024* [Technical report].

NCHM. (2025a). *Annual glacier mass balance on Shodug Glacier, 2024–2025* [Technical report].

NCHM & ICIMOD. (2025). *First seasonal glacier mass balance measurement in Bhutan: A joint initiative of NCHM and ICIMOD* [Field report].

O'Neel, S., McNeil, C., Sass, L. C., Florentine, C., Baker, E. H., Peitzsch, E., McGrath, D., Fountain, A. G., & Fagre, D. B. (2019). Reanalysis of the US Geological Survey benchmark glaciers: Long-term insight into climate forcing of glacier mass balance. *Journal of Glaciology, 65*(253), 850–866. https://doi.org/10.1017/jog.2019.66

Tshering, P., & Fujita, K. (2016). First in situ record of decadal glacier mass balance (2003–2014) from the Bhutan Himalaya. *Annals of Glaciology, 57*(71), 289–294. https://doi.org/10.3189/2016AoG71A036

WMO. (2025). *State of the global climate 2025*. World Meteorological Organization.

Zemp, M., Huss, M., Thibert, E. *et al.* Global glacier mass changes and their contributions to sea-level rise from 1961 to 2016. *Nature* **568**, 382–386 (2019). https://doi.org/10.1038/s41586-019-1071-0

8 Annexes

8.1 Annex A: Hypsometric elevation-band statistics and point mass balance

Tables A1 and A2 summarize elevation-band (hypsometric) elevation differences (Δh), derived areas, perimeter, and point mass balance outputs used in the geodetic mass balance workflow for annual and seasonal mass balance.

Table A1. Annual elevation-band statistics.

Elevation band (m a.s.l.)	Mid-elevation (m)	Pixel count	Mean Δh (m)	Mean band area (m²)	Area (%)	Perimeter (m)	Point mass balance (mm w.e.)	Area-weighted MB contribution (mm w.e.)	Uncertainty (Ice)	Uncertainty (Snow)
5116-5166 m	5141	1717	-2.509	116163.06	10.46698	1179.748	-2565.29	-268.182	30.094	37.719
5166-5216 m	5191	2759	-2.007	343966.091	30.99337	1220.811	-2136.18	-649.003	85.526	107.325
5216-5266 m	5241	1732	-1.639	313192.18	28.22046	842.362	-1707.07	-491.818	75.603	95.216
5266-5316 m	5291	801	-1.394	222814.952	20.07694	879.45	-1277.95	-301.388	53.579	67.513
5316-5366 m	5341	676	-0.563	61674.638	5.557248	378.359	-848.843	-41.287	14.786	18.7
5366-5416 m	5391	0	-0.226	47175.391	4.250781	423.425	-419.732	-17.842	10.599	13.41
5416-5466 m	5441	0	0.231	4818.992	0.43422	243.578	9.38	0.041	1.143	1.447
Total				**1109805.30**				**-1769.48**		

Table A2. Seasonal elevation-band statistics.

Elevation band (m a.s.l.)	Mid-elevation (m)	Pixel count	Mean Δh (m)	Mean band area (m²)	Area (%)	Perimeter (m)	Point mass balance (mm w.e.)	Area-weighted MB contribution (mm w.e.)	Uncertainty (Ice)	Uncertainty (Snow)
5116-5166 m	5141	2162	0.387	118699.371	10.69551	1179.748	173.152	18.519	5.237	12.863
5166-5216 m	5191	2842	0.279	343120.654	30.91719	1220.811	124.609	38.526	14.903	36.702
5216-5266 m	5241	1847	0.185	312769.461	28.18237	842.362	88.089	24.826	13.312	32.925
5266-5316 m	5291	934	-0.062	223026.311	20.09599	879.45	−82.615	-16.602	9.456	23.39
5316-5366 m	5341	754	0.324	60195.123	5.423935	378.359	304.400	16.51	2.666	6.58
5366-5416 m	5391	0	-0.099	47175.391	4.250781	423.425	−21.870	-0.93	1.896	4.706

5416-5466 m	5441	0	-0.194	4818.992	0.43422	243.578	−58.473	-0.254	0.205	0.509
Total				**1109805.30**				**80.595**		

8.2 Annex B: Physical assumptions

Densities used

The following densities were applied for the geodetic mass balance measurement:

- **Ice density:** i≈880 kg m-3
- **Snow density:** s≈400 kg m-3
- **Water density:** w≈1000 kg m-3

8.3 Annex C: Unit equivalence used in mass-balance calculations

In glacier mass-balance studies, mass changes are commonly expressed either as mass per unit area (kg m^{-2}) or as millimetres of water equivalent (mm w.e.). These two units are directly and numerically equivalent due to the physical relationship between mass, area, thickness, and the density of liquid water.

Mass balance expressed in kg m^{-2} represents the amount of mass gained or lost per square meter of glacier surface. When this mass is converted to an equivalent thickness of water, the relationship is given by:

$$h = \frac{m}{\rho_w}$$

where

h= equivalent water thickness (m),

m= mass per unit area (kg m^{-2}), and

ρ_w= density of liquid water (≈ 1000 kg m^{-3}).

For a mass change of 1 kg m^{-2}:

$$h = \frac{1\, kg\, m^{-2}}{1000\, kg\, m^{-3}} = 0.001\, m = 1\, mm$$

Thus, a mass of 1 kg uniformly distributed over an area of 1 m^2 corresponds to a water layer of 1 mm thickness. This leads to the direct numerical equivalence:

1 kg m^{-2} = 1 mm w.e.

As a result, glacier mass-balance values reported in kg m^{-2} can be directly expressed in millimetres of water equivalent without further scaling, provided the reference density is that of liquid water. This convention allows glacier mass changes to be interpreted intuitively as an equivalent water depth and facilitates comparison across glaciers of different sizes.

8.4 Annex D: Snow and ice density uncertainty in mass-balance calculations

In the conversion of elevation change to mass balance, assumed densities for glacier ice and snow introduce an additional source of uncertainty. These densities are not constant; they vary spatially and temporally due to differences in internal structure, compaction, temperature, and metamorphic processes. To account for this variability, density-related uncertainties were explicitly included in the uncertainty propagation. Reference densities for glacier ice and snow were adopted as specified in Annex C. For the current study, seasonal snow was present during the survey period and was explicitly incorporated through the $\Delta S(z)$ term; therefore, uncertainty contributions from both ice and snow densities were included in the final uncertainty calculation. Density uncertainties of ± 30 kg m^{-3} (ice) and ± 100 kg m^{-3} (snow) were applied following common ranges reported in glaciological studies and consistent with the workflow implementation.

NATIONAL CENTRE FOR HYDROLOGY AND METEOROLOGY

ROYAL GOVERNMENT OF BHUTAN

www.nchm.gov.bt